iScience

CellPress
OPEN ACCESS

Article

ICAM1 antibody drug conjugates exert potent antitumor activity in papillary and anaplastic thyroid carcinoma

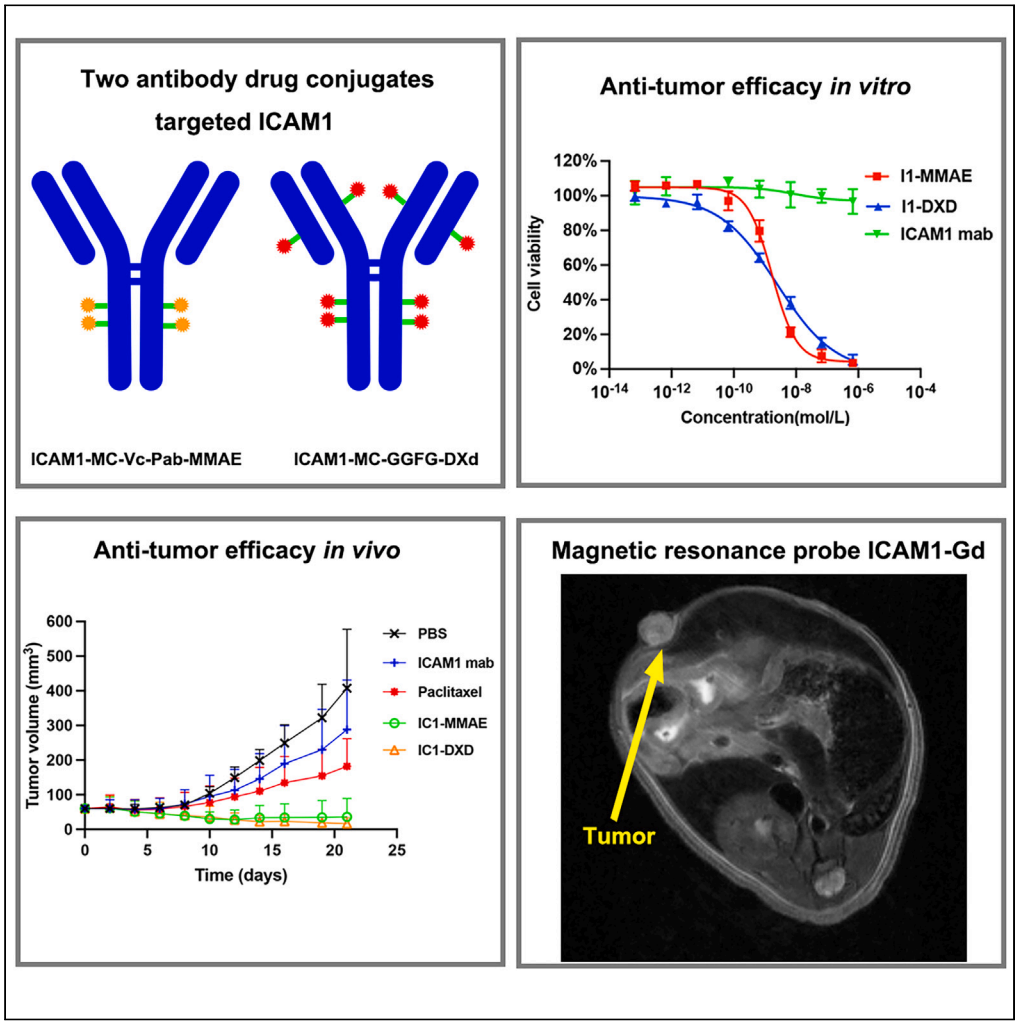

Peng Zhang, Changjuan Tao, Takaya Shimura, ..., Jianmin Fang, Marsha A. Moses, Peng Guo

jfang@tongji.edu.cn (J.F.)
marsha.moses@childrens.harvard.edu (M.A.M.)
guopeng@ucas.ac.cn (P.G.)

Highlights

ICAM1 was identified as a target of antibody drug conjugate in thyroid cancer

Two ICAM1 antibody drug conjugates showed anti-tumor efficacy *in vitro* and *in vivo*

A noninvasive MRI probe (ICAM1-Gd) was designed to develop precision medicine

Zhang et al., iScience *26*, 107272
August 18, 2023
https://doi.org/10.1016/j.isci.2023.107272

iScience

CellPress
OPEN ACCESS

Article

ICAM1 antibody drug conjugates exert potent antitumor activity in papillary and anaplastic thyroid carcinoma

Peng Zhang,[1,2,3,13] Changjuan Tao,[2,3,4,13] Takaya Shimura,[5] Andrew C. Huang,[6] Nana Kong,[6] Yujie Dai,[6] Shili Yao,[7] Yun Xi,[8] Xing Wang,[9] Jianmin Fang,[10,14,*] Marsha A. Moses,[11,12,14,*] and Peng Guo[3,14,15,*]

SUMMARY

Treatment options for anaplastic thyroid cancer (ATC) and refractory papillary thyroid carcinoma (PTC) are limited and outcomes remain poor. In this study, we determined via bioinformatic expression analyses and immunohistochemistry staining that intercellular adhesion molecule-1(ICAM1) is an attractive target for ATC and PTC. We designed and engineered two ICAM1-directed antibody-drug conjugate (I1-MMAE and I1-DXd), both of which potently and selectively ablate multiple human ATC and PTC cell lines without affecting non-plastic cells *in vitro*. Furthermore, I1-MMAE and I1-DXd mediated a potent tumor regression in ATC and PTC xenograft models. To develop a precision medicine, we also explored magnetic resonance imaging (MRI) as a non-invasive biomarker detection method to quantitatively map ICAM1 antigen expression in heterogeneous thyroid tumors. Taken together, this study provides a strong rationale for the further development of I1-MMAE and I1-DXd as promising therapeutic candidates to treat advanced PTC and ATC.

INTRODUCTION

Thyroid cancer is the most common endocrine malignancy diagnosed worldwide with 586,202 new cases and 43,646 new deaths in 2020.[1] Thyroid cancer has been the third most prevalent cancer among females in United States in 2022.[2] Thyroid cancer can be classified into differentiated thyroid cancer (papillary thyroid cancer and follicular thyroid cancer), poorly differentiated thyroid carcinoma, and anaplastic thyroid carcinomas (ATC), while papillary thyroid cancer (PTC) represents the most common subtype of thyroid cancers, accounting for over 85% of all cases. To date, standard chemotherapy has limited efficacy in advanced PTC and ATC. Approximately 10% of advanced PTC patients relapse, develop radioactive iodine resistance and distant metastases leaving limited therapeutic options. ATC, as one of the most aggressive cancers, is almost uniformly lethal with a median overall survival (OS) time of 3–6 months and a 5-year survival rate of less than 5%,[3] highlighting a significant unmet need for improving the clinical outcomes of advanced PTC and ATC patients.

Recent therapeutic strategies have employed kinase inhibitors such as sorafenib and lenvatinib as the main targeted treatment for advanced PTC patients. However, neither trial of these two therapeutics showed a statistically significant difference in overall survival.[4,5] Though BRAF inhibitors with or without MEK inhibitor have been used to treat BRAF-mutated thyroid cancers,[6,7] only a small subset of ATC patients carries a $BRAF^{V600E}$ (20–30%) and may benefit. For these reasons, an urgent and unmet clinical need exists to discover drug targets and more effective targeted therapeutics for advanced PTC and ATC.

Antibody-drug conjugates (ADCs) are an emerging therapeutic modality demonstrating promising efficacy against various refractory and metastatic solid tumors including gastric and certain breast cancers. For example, trastuzumab deruxtecan, a HER2-targeted ADC, improved the median overall survival by 6.6 months in HER2-low metastatic breast cancer patients in comparison with standard chemotherapy in the Phase III DESTINY-Breast04 clinical trial.[8] Such ADC consists of a monoclonal antibody (mAb) conjugated to a cytotoxic agent (payload) via a cleavable chemical linker in response to tumor microenvironments, providing a therapeutic advantage by selectively killing tumor cells while sparing normal tissues from collateral damages.[9] Moreover, ADCs can readily overcome acquired drug resistances by switching their payloads to other cytotoxic agents with different mechanisms of actions such as from microtubule

[1]Department of Medical Oncology, The Cancer Hospital of the University of Chinese Academy of Sciences, Zhejiang Cancer Hospital, Hangzhou, Zhejiang 310022, China

[2]Key Laboratory of Head and Neck Cancer Translational Research of Zhejiang Province, Zhejiang Cancer Hospital, Hangzhou, Zhejiang 310022, China

[3]Institute of Basic Medicine and Cancer (IBMC), Chinese Academy of Sciences, Hangzhou, Zhejiang 310022, China

[4]Department of Radiation Oncology, The Cancer Hospital of the University of Chinese Academy of Sciences, Zhejiang Cancer Hospital, Hangzhou, Zhejiang 310022, China

[5]Department of Gastroenterology and Metabolism, Nagoya City University Graduate School of Medical Sciences, Nagoya 467-8601, Japan

[6]MabPlex International, Yantai, Shandong 264006, China

[7]School of Materials Science and Engineering, Tianjin University, Tianjin 300072, China

[8]Department of Pathology, The Cancer Hospital of the University of Chinese Academy of Sciences, Zhejiang Cancer Hospital, Hangzhou, Zhejiang 310022, China

[9]Department of Head and Neck Surgery, The Cancer Hospital of the University of Chinese Academy of Sciences, Zhejiang Cancer Hospital, Hangzhou, Zhejiang 310022, China

[10]School of Life Science and Technology, Tongji University, Shanghai 200092, China

Continued

inhibitors (e.g., MMAE) to DNA topoisomerase inhibitors (e.g., DXd). Currently, there is no clinically effective ADCs for advanced PTC and ATC owing to the lack of effective targets.

Intercellular adhesion molecule-1 (ICAM1) is a transmembrane glycoprotein receptor located on the cell surface. Previous studies have revealed that ICAM1 played an important role in tumor carcinogenesis, tumorigenesis and initiation of tumor metastasis.[10] The upregulation of ICAM1 expression was reported in several malignancies, including aggressive thyroid cancer,[11–13] triple-negative breast cancer,[14] and pancreatic cancer.[15] Previous study also revealed that higher ICAM1 expression indicated poor prognosis and was significantly correlated with tumor aggressiveness markers in thyroid cancer, including BRAF mutation, lymph node metastasis, and poorly differentiation.[12,13] Notably, Jin et al. developed a series of CAR-T cell therapy targeting ICAM1 that exhibited therapeutic efficacy against multiple solid tumors including advanced ATC in animal models and CAR-T cell therapy targeting ICAM1 has entered phase I clinical trial (clinical trial information: NCT04420754).[13,16–18] In this study, we performed an unbiased bioinformatic screening with systematic drug target evaluation to identify ICAM1 as a rational ADC target for advanced PTC and ATC. Two proof-of-concept ICAM1 ADCs were developed by utilizing different cleavable linkers and cytotoxic payloads with different anticancer mechanisms and therapeutic efficacy was quantitatively evaluated and compared *in vivo*. Moreover, we utilized a magnetic resonance (MRI)-based molecular imaging approach to noninvasively identify target positive tumors suitable for ADC therapy,[15] representing an opportunity to develop a precision medicine for PTC and ATC therapy.

RESULTS

Identification of ICAM1 as a potential ADC target for advanced PTC and ATC

We obtained gene expression date from Gene Expression Omnibus (GEO, http://www.ncbi.nlm.nih.gov/geo/); the GEO accession number is GSE3467, GSE33630, and GSE50901. A total of 183, 330, and 172 differential expressed genes (DEGs) (|logFC|>1.8 and adjust p value < 0.05) were identified from GSE3467, GSE33630, and GSE50901, respectively (Figures 1A and S1A) and 47 DEGs were screened out from all 3 datasets as shown in Figure 1A. To further explore the interactions among proteins encoded by common identified DEGs, a protein-protein interaction (PPI) network was constructed according to the STRING database (Figure S1B). Subsequently, the top 10 DEGs with higher degrees were screened and selected as hub genes with Cytoscape plug-in cytohubba (Figures 1B and S1C). Among these hub genes, ICAM1 ranked first in five calculations methods (Figures 1B, S1C and Table S1).

The overexpression of ICAM1 in PTC was further validated using a TCGA dataset (505 thyroid cancer patients and 59 normal patients) and ATC samples. The transcriptomic expression level of ICAM1 was significantly increased in thyroid cancer tissues in comparison with normal thyroid tissues (Figure 1C). We also found that the tall-cell variant (TCV) of papillary thyroid carcinoma (PTC), as more aggressive subtype of PTC with poorer prognosis, exhibited a higher expression level of ICAM1 than conventional PTC (p = 1.62e-12, Figure 1D). Importantly, the expression level of ICAM1 also significantly increased with lymph node metastasis (N0 vs. Normal: p = 1.62e-12, N1 vs. N0: p = 7.98e-4; Figure 1E), indicating it may be a potential drug target for advanced thyroid cancers. It is important to note that ICAM1 expression was similar between male and female patients (p = 0.672, Figure 1F). Thyroid differentiation, which plays a central role in thyroid cancer progression, was evaluated using a thyroid differentiation score (TDS) designed by the expression level of 16 thyroid metabolism and function genes (Table S2).[19] In the TCGA thyroid cancer cohort, ICAM1 expression level was significantly negatively correlated with TDS (Spearman R = −0.51, p = 5.12e-36, Figure 1G), indicating that ICAM1 overexpression represents a poorer disease differentiation associated with worse clinical outcomes. ICAM1 expression level also positively correlates with Ki67 levels, a classic cell proliferation marker (Spearman R = 0.44, p = 7.5e-36, Figure 1H). Furthermore, multiple studies including the TCGA study revealed that nonoverlapping alterations within MAPK signaling pathway dominated in thyroid cancer and that mutant BRAF, RAS, RET fusions contributed to approximately 80% of known alterations in PTCs.[20] Therefore, the MAPK pathway is a key molecular pathway associated with the onset and progression of thyroid cancer. The MAPK Pathway Activity Score (MPAS), which aggregated gene expression measurements from 10 highly conserved MAPK transcription targets (Table S2), could represent the extent of pathway activity better than single gene mutation status.[21] The ICAM1 expression level was significantly positively associated with MPAS (Spearman R = 0.61, p = 3.5e-53, Figure 1I). Consistently, the thyroid cancer patients with ICAM1-high expression exhibit a significantly worse disease-free survival (DFS) (log rank p = 0.025, Figure 1J) in comparison with those with ICAM1-low expression. Subsequently, the ICAM1 overexpression was also validated in the ATC

[11]Vascular Biology Program, Boston Children's Hospital, Boston, MA 02115, USA

[12]Department of Surgery, Boston Children's Hospital and Harvard Medical School, Boston, MA 02115, USA

[13]These authors contributed equally

[14]These authors contributed equally

[15]Lead contact

*Correspondence: jfang@tongji.edu.cn (J.F.), marsha.moses@childrens.harvard.edu (M.A.M.), guopeng@ucas.ac.cn (P.G.)

https://doi.org/10.1016/j.isci.2023.107272

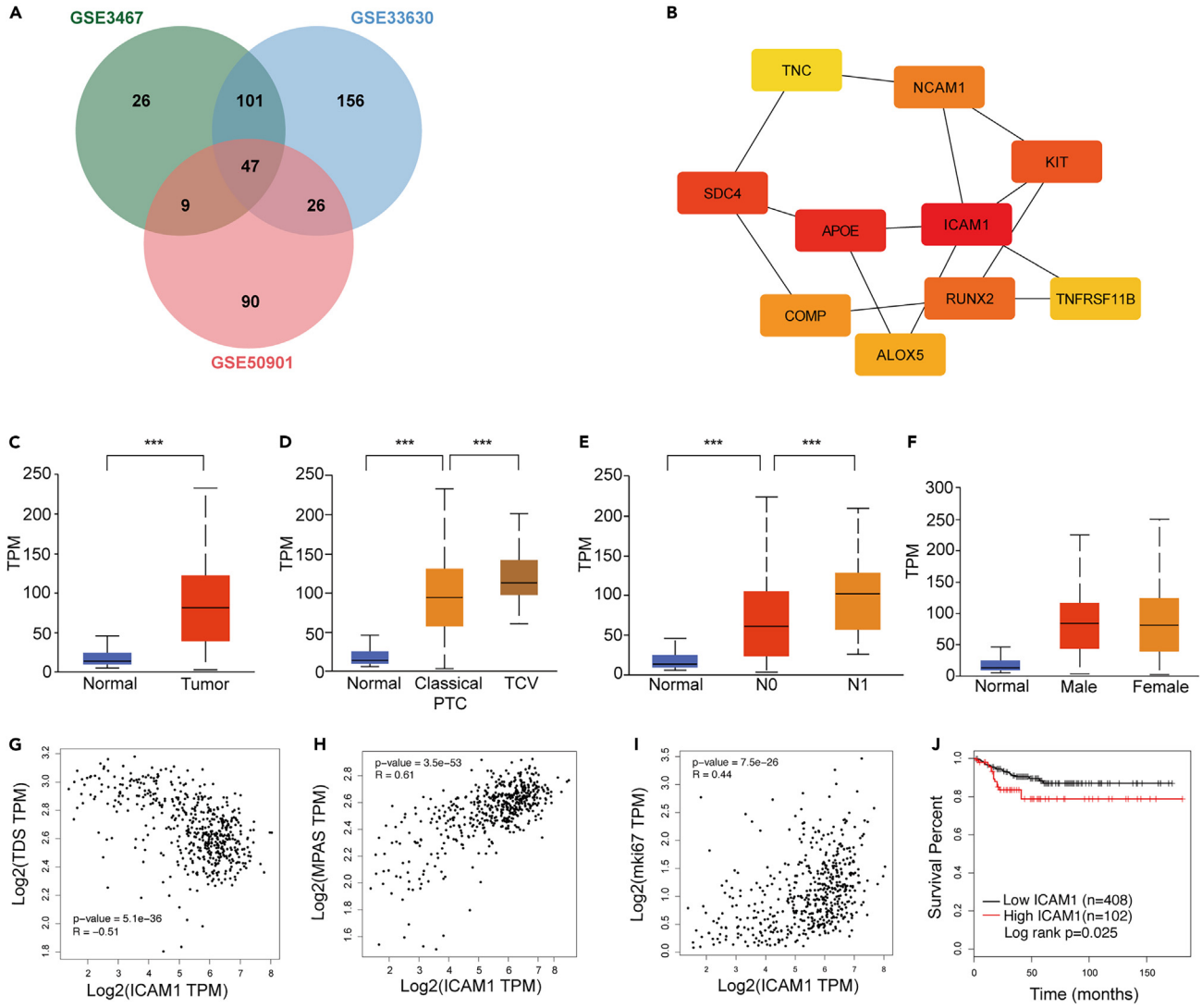

Figure 1. ICAM1 was identified as an attractive target for PTC and ATC

(A) Venn diagram of differentially expressed genes in PTC gene expression profiling datasets.

(B) Hub genes identified by cytoscape with Edge Percolated Component (EPC) method.

(C) Boxplots compare ICAM1 mRNA levels via thyroid cancer to normal thyroid tissue.

(D) Boxplots compare ICAM1 mRNA levels via normal thyroid tissue, classical PTC to tall PTC.

(E) Boxplots compare ICAM1 mRNA levels via normal thyroid tissue, absence of lymph node metastasis to presence of lymph node metastasis.

(F) Boxplots compare thyroid cancer ICAM1 mRNA levels via male to female.

(G–I) Spearman correlation analysis between ICAM1 mRNA expression and thyroid differentiation score (G), Ki67(H) and MAPK pathway activity score (I).

(J) Kaplan-Meier analysis of disease free survival of thyroid cancer patients according to different ICAM1 levels in TCGA cohort. Students' T test was employed in (C–E); ***p < 0.001.

GEO datasets (GSE33630, GSE53072, and GSE65144). ICAM1 was overexpressed in all ATC GEO datasets (Figure S2B). Notably, ICAM1 mRNA levels in ATC samples were significantly high than PTC and normal thyroid in the same GEO dataset (GSE33630) (Figure S2C).[22] To validate aforementioned transcriptomic findings at the protein level, we performed an IHC staining of ICAM1 in tissue microarray (TMA). The IHC results revealed that immunostaining of ICAM1 was predominantly membranous staining (Figure 2A). Normal thyroid tissue samples had no/low expression of ICAM1. All of ATC overexpressed ICAM1. As is shown in Figure 2B, the IHC H-score in ATC was significantly higher than that of PTC and normal thyroid tissue (PTC vs. Normal: $p < 0.001$; ATC vs. PTC: $p = 0.029$). These findings confirmed and extended previous study[13] that ICAM1 was a potential target candidate for advanced PTC and ATC.

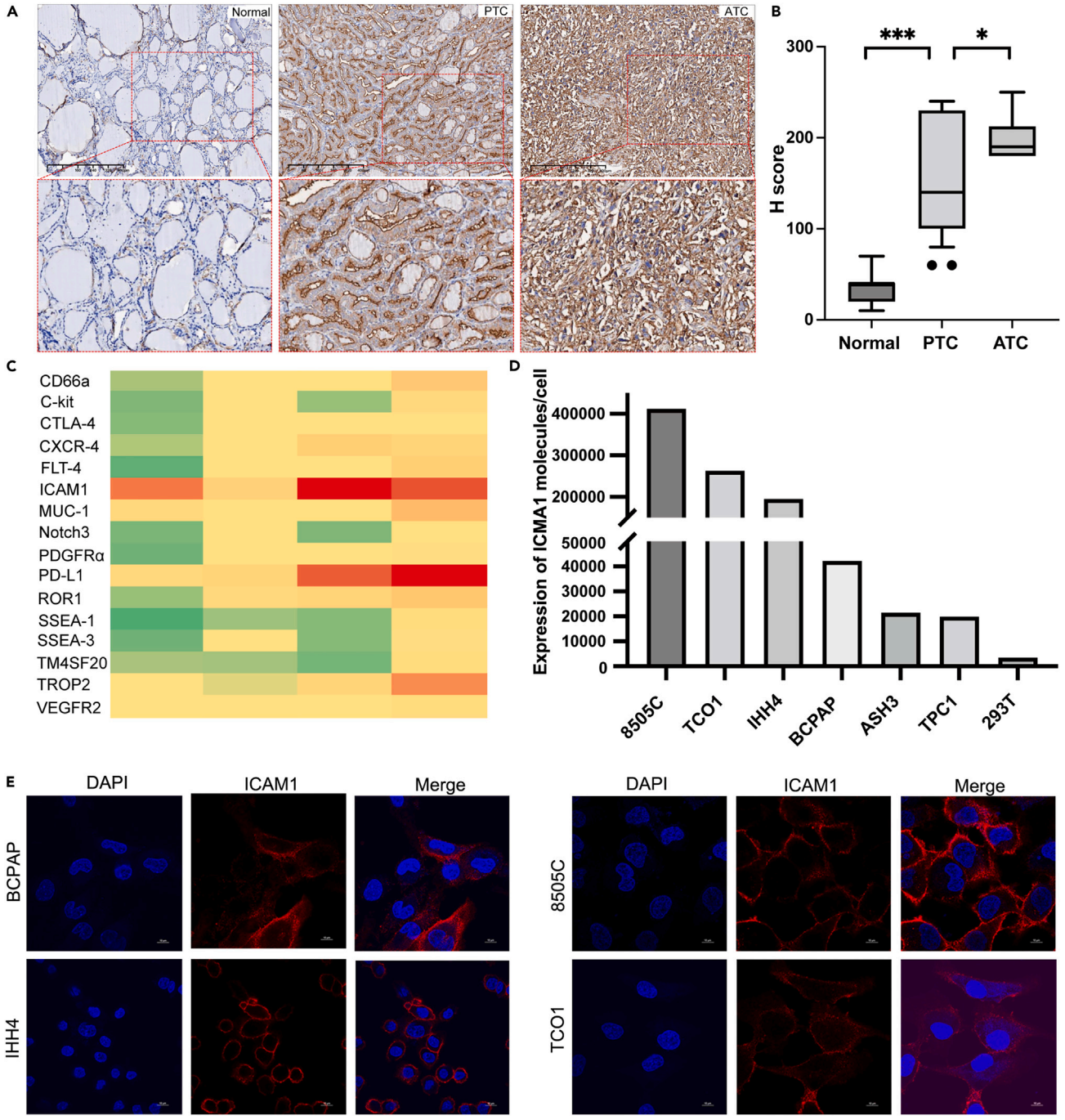

Figure 2. ICAM1 is overexpressed in thyroid cancer

(A) Representative images of IHC staining of ICAM1 in human normal thyroid tissue, PTC and ATC.

(B) Boxplots compare H-score of ICAM1 IHC via normal thyroid tissue, PTC to ATC; Bar graphs are shown as mean ± SD. One-way ANOVA was employed; *$p < 0.05$; ***$p < 0.001$.

(C) Heatmap of membrane proteins expression in human thyroid cancer cells.

(D) Representative flow cytometry plots showing ICAM1 expression in PTC (BCPAP, IHH4, TPC-1), ATC (8505C, TCO1, ASH3) cell lines and normal 293T cell.

(E) IF staining of ICAM1 in PTC and ATC cells.

To compare ICAM1 with other established targets for thyroid cancer, we performed a quantitative and unbiased screening of 16 thyroid cancer-related antigens in four human PTC and ATC cell lines (BCPAP, IHH4, 8505C, and TCO1). As depicted in the heatmap (Figure 2C), the common top 5 most overexpressed antigens in at least 3 cell lines were identified as ICAM1, PD-L1, TROP2, and MUC1 (Table S3) with ICAM1 emerging as the uniformly overexpressed candidate in all four screened PTC and ATC cell lines (Figure 2D). We also quantified the surface density of ICAM1 as 412,023 (8505c); 263,176(TCO1); 194,993(IHH4); 42,211(BCPAP); 21,514(ASH3); and 19,948(TPC1), respectively (Figure 2D). In comparison, ICAM1 expression of normal human epithelial 293T was undetectable (Figure 2D). The ICAM1 overexpression on the cytoplasmic membrane was directly visualized on human PTC and ATC cells by immunofluorescent staining (Figures 2E and 2F).

Given that antigen-mediated internalization can directly impact ADC therapeutic efficacy and is considered as a requisite for ADC targets,[23] we evaluated antigen-mediated internalization of ICAM1 antibody via two independent approaches: time-dependent flow cytometry and IF staining. The IF staining imaging showed that the fluorescent PE-conjugated ICAM1 antibodies initially bound on cytoplasmic membrane of PTC (IHH4) and ATC (8505C) cells at the 10 min incubation time, and were gradually internalized into the endosomes and lysosomes of PTC and ATC cells via antigen-mediated endocytosis with incubation time (Figure 3A). We next quantified internalization curves of ICAM1 antibodies in human thyroid cancer cells by flow cytometry (Figure 3B). At 4 h post-incubation, internalization rates of ICAM1 antibodies reached a plateau of 27.4% (BCPAP), 19.4% (IHH4), 32.1% (8505C), and 25.9% (TCO1) in human thyroid cancer cells, respectively. These findings demonstrate that ICAM1 can be potentially used as a drug delivery target for developing ADCs for advanced PTC and ATC.

Design and synthesis of ICAM1 ADCs with different linkers and payloads

Various ADC linker and payload combinations have been clinically approved for treating solid tumors, yet no quantitative analysis of their efficacy has been conducted in PTC and ATC. To identify the optimal ADC formulation for advanced PTC and ATC, we engineered two ICAM1 ADCs by conjugating monoclonal ICAM1 antibodies with two clinically proven chemical linker and payload combinations: MC-Vc-Pab-MMAE or MC-GGFG-DXd (Figure 4A).[24] Both of these are enzyme-cleavable in cell endosomes/lysosomes upon internalization. DARs of I1-MMAE and I1-DXd were 4 and 8, respectively.

We next determined the *in vitro* cytotoxicity of I1-MMAE and I1-DXd by quantifying their half maximum inhibitory concentrations (IC_{50}) in human thyroid cancer cells. For PTC cells (IHH4 and BCPAP), the IC_{50} of I1-MMAE were determined as 1.69 $\pm$ 0.31 nM and 68.6 $\pm$ 11.2 nM, whereas I1-DXd exhibit a similar IC_{50} of 2.48 $\pm$ 0.88 nM and 54.1 $\pm$ 19.4 nM, respectively. Both ICAM1 ADCs also exhibited similar IC_{50} in ATC cells (TCO1 and 8505C), which IC_{50} were determined as 15.59 $\pm$ 4.18 nM and 7.35 $\pm$ 1.45 nM for I1-MMAE. It is noteworthy that the IC_{50} of I1-MMAE was significantly lower than paclitaxel in all four thyroid cancer cells treated, which is currently recommended to treat advanced thyroid cancer by NCCN guideline. Non-neoplastic 239T cells were selected as an ICAM1-negative control and I1-MMAE and I1-DXd did not show any cytotoxicity in 293T cells due to the lack of ICAM1 expression.

ICAM1 ADCs exhibit high tumor-specificity and limited biodistribution

We evaluated the tumor specificity and biodistribution of ICAM1-ADCs by *in vivo* NIR fluorescent imaging as previously reported by us.[25] Subcutaneous ATC tumor (8505C) bearing mice were injected with near-infrared fluorescent dye Cy5.5 labeled anti-human I1-MMAE (I1-MMAE-Cy5.5) and non-targeting IgG conjugated with Cy5.5 (IgG-Cy5.5) at an equivalent dosage of 5 mg/kg and animals were imaged at 48 h post-injection *in vivo*. As is shown in Figures 5A–5C, the tumor accumulation of I1-MMAE-Cy5.5 was approximately 2.2-fold higher than non-targeting controls, which precisely matched the *ex vivo* NIR images of excised tumors. These results suggest that I1-MMAE-Cy5.5 selectively recognize and bind thyroid tumors *in vivo* relative to the non-targeting group (IgG-Cy5.5). In addition, we also examined the biodistribution of vital organs (brain, heart, lung, spleen, liver, and kidney). As is shown in Figures 5 B and 5D, the accumulation of I1-MMAE-Cy5.5 in six normal organs was similar to the non-targeting IgG-Cy5.5 group, where liver is a major off-tumor accumulation site for ICAM1 ADCs.

Therapeutic potential of ICAM1 ADCs in PTC and ATC

We utilized two subcutaneous xenograft mouse models for PTC (IHH4 cell) and ATC (8505C cell) to evaluate the *in vivo* efficacy of ICAM1-ADCs. Treatment with I1-MMAE or I1-DXd was initiated at the intravenous (i.v.)

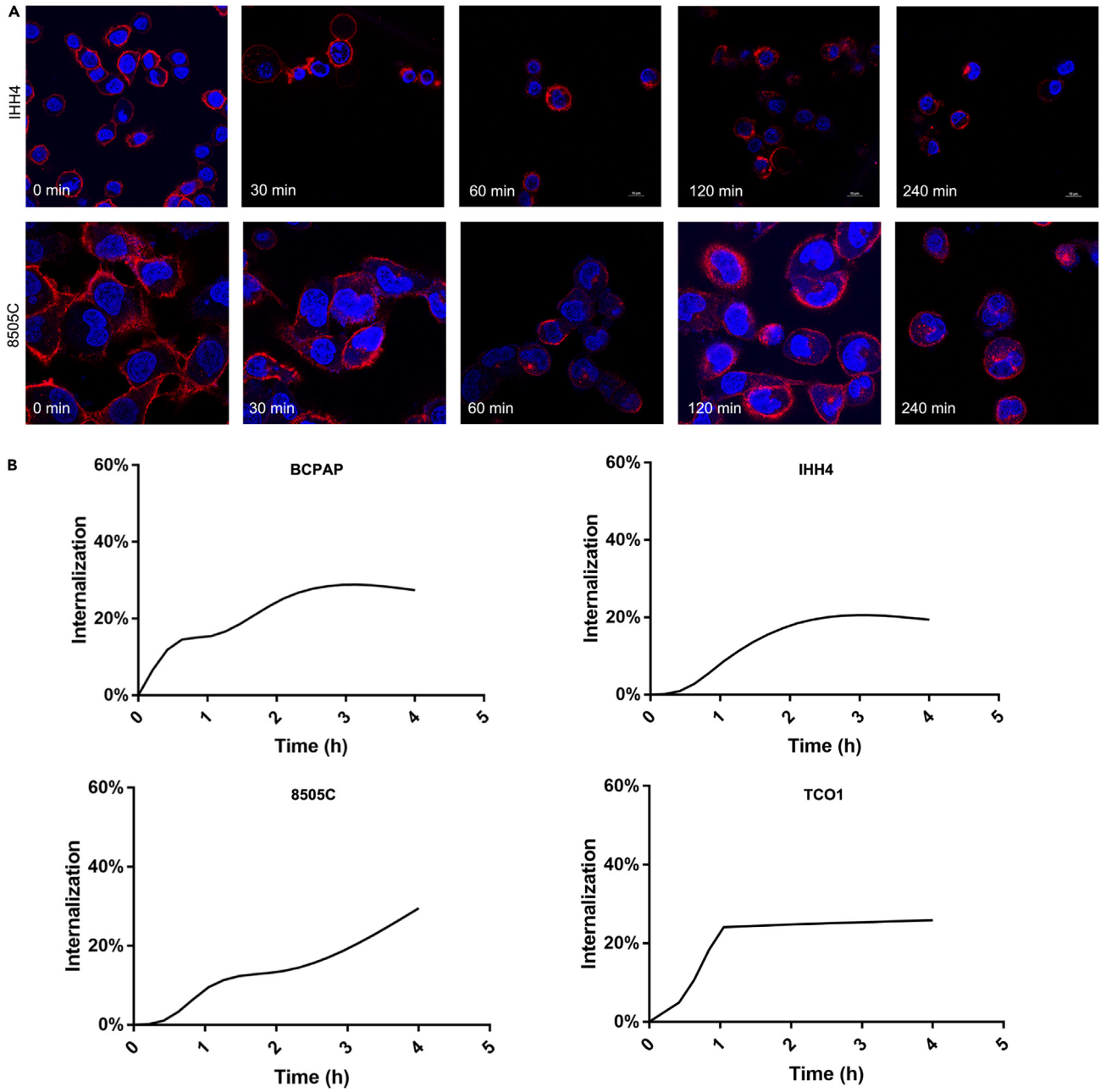

Figure 3. PE-conjugated ICAM1 antibodies was significantly internalized by PTC and ATC cells

(A) Internalization curve of ICAM1 in PTC and ATC cells quantified by flow cytometry.

(B) Representative images of IF staining of ICAM1 internalization in different time point (0min, 30min, 60min, 120min, 240min) in PTC cell (IHH4) and ATC cell (8505C).

dosage of 5 mg/kg/week via tail vein injection. Separate subgroups of tumor-bearing mice were treated with PBS (sham) or ICAM1 antibody alone or paclitaxel as controls at same dosage and schedule. In the PTC mouse model, both I1-MMAE and I1-DXd showed significant and durable tumor regression in every animal tested throughout the duration of the experiment (Figure 6). The mean tumor size of terminal tumor in I1-MMAE and I1-DXd groups were significantly smaller than those of PBS groups ($p = 0.003$; $p = 0.001$; respectively). The mean tumor size in I1-DXd group was also slightly smaller than those of I1-MMAE group, but this difference was not significant ($p = 0.469$). The mean tumor weight in each group were quantified as 0.76 ± 0.51 g (PBS), 0.79 ± 0.45 g (ICAM1 antibody), 0.58 ± 0.18 g (paclitaxel), 0.15 ± 0.07 g (I1-MMAE),

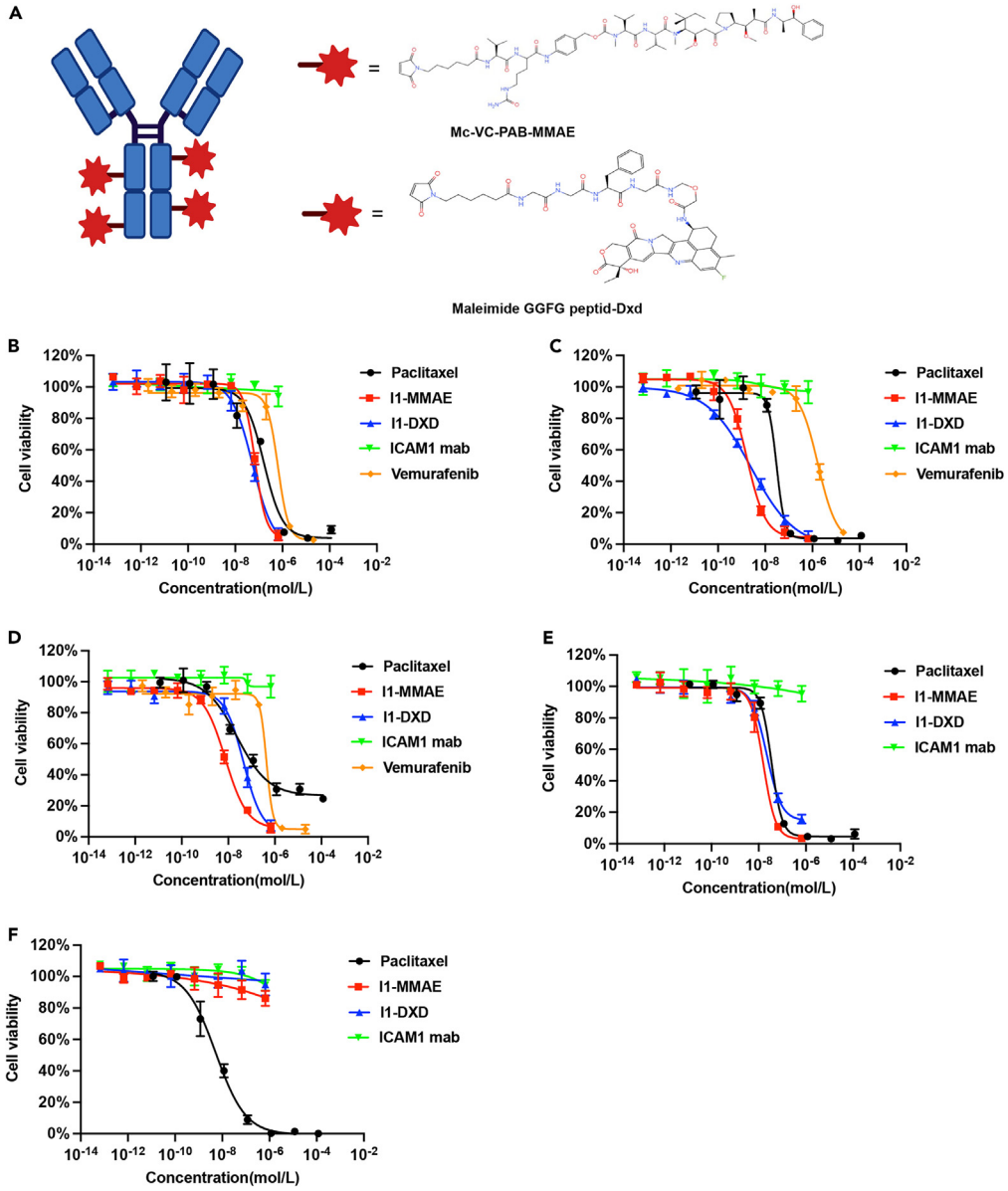

Figure 4. *In vitro* anti-tumor cytotoxicity analysis of ICAM1-ADCs

(A) Schematic illustration and chemical structures of ICAM1-ADC linkers and warheads.

(B–F) *in vitro* cell growth inhibitory activity in BCPAP(B), IHH4(C), 8505C(D), TCO1(E), and 293T cell (F), The cells were treated with ICAM1 antibody, I1-MMAE, I1-DXd paclitaxel and vemurafenib (in BRAF mutation cells). Each point represents the mean and SD (n = 3).

and 0.07 ± 0.02 g (I1-DXd), respectively (Figure 6C). No obvious bodyweight difference was observed among the five treatment groups (Figure 6D), suggesting that ADCs were well tolerated.

We observed a similar efficacy of I1-MMAE and I1-DXd in a more aggressive ATC model generated from 8505C cells. The tumor size significantly shrank by over 95% and 89% after I1-DXd and I1-MMAE treatment ($p < 0.001$; $p < 0.001$; respectively). Strikingly, 20% of ATC tumors were completely eradicated upon I1-MMAE or I1-DXd treatments (Figure 6E), whereas I1-DXd exhibit an improved efficacy in comparison with I1-MMAE ($p = 0.777$). No significant body weight loss in each group was observed (Figure 6H). Based on these *in vivo* efficacy results, we selected I1-DXd as the optimized ICAM1 ADC formation for advanced PTC and ATC therapy. To evaluate the potential systemic toxicity of ADC, the major organs in 8505C

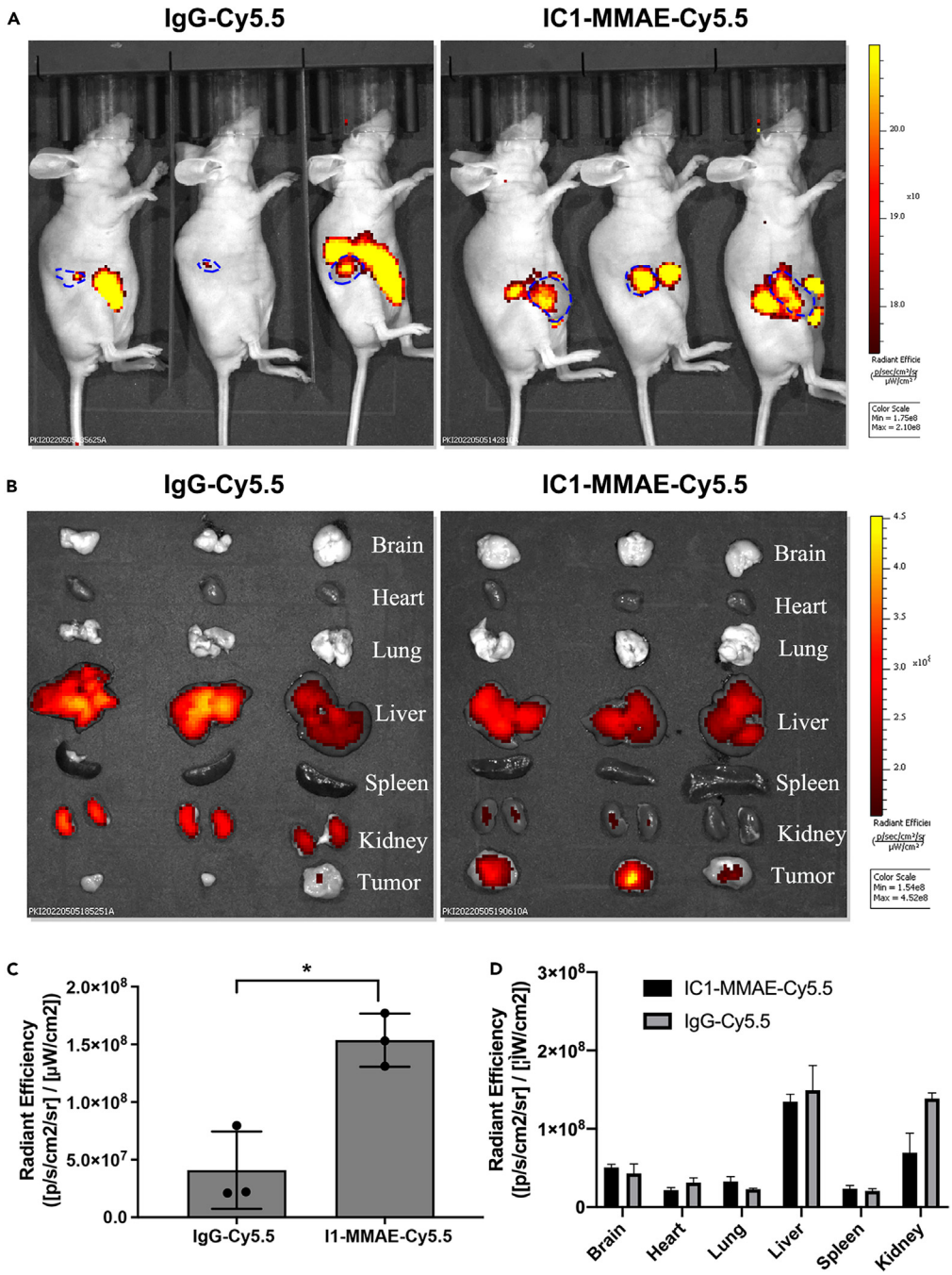

Figure 5. Tumor-specificity and biodistribution of ICAM1-ADC in nude mice

(A) *in vivo* NIR fluorescent images of nude mice at 48h after the administration of IgG-Cy5.5 or I1-MMAE-Cy5.5.

(B) Representative *ex vivo* NIR fluorescent images of six major organs including brain, lung, heart, spleen, liver, and kidney.

(C) Quantified tumor accumulation of IgG-Cy5.5 or I1-MMAE-Cy5.5; Students' T test was employed to compare difference; *$p < 0.05$.

(D) Quantified normal major organ accumulation of IgG-Cy5.5 or I1-MMAE-Cy5.5.

subcutaneous tumor model, such as heart, lung, kidney, liver, spleen, and kidney were analyzed after HE staining. As shown in Figures 6G and S3C, no obvious difference in the morphology of these organs were observed among groups. Besides, no necrosis or degenerative changes were identified in I1-DXd

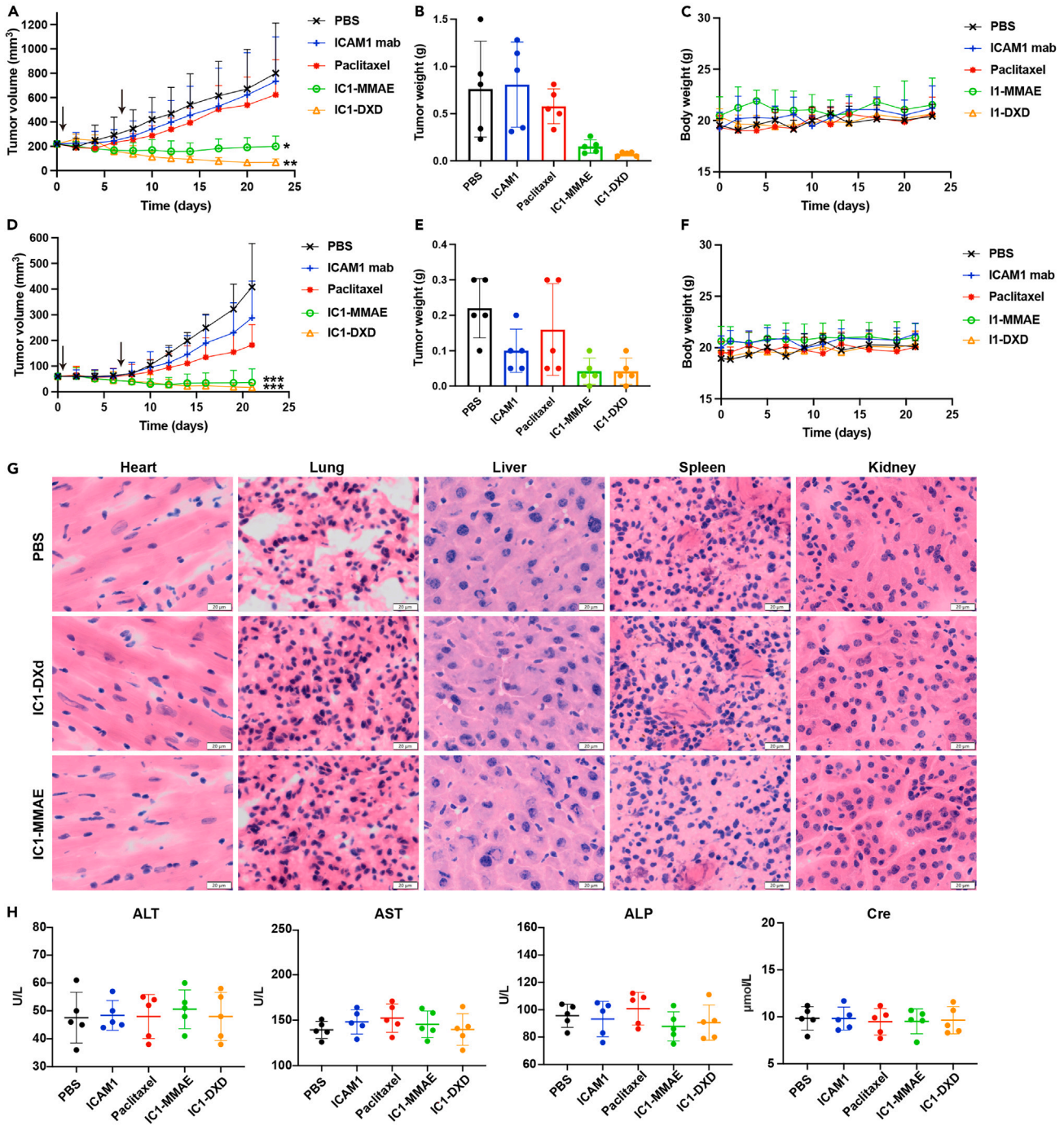

Figure 6. ICAM1-ADCs eradicate PTC and ATC tumors *in vivo*

(A) Tumor progression in subcutaneous IHH4 tumors by tumor volume measurement by caliper.

(B) Tumor mass at endpoint of subcutaneous IHH4 tumors were quantified by weight.

(C) Mouse body weights of subcutaneous IHH4 tumors.

(D) Tumor progression in subcutaneous 8505C tumors by tumor volume measurement by caliper.

(E) Tumor mass at endpoint of subcutaneous 8505C tumors were quantified by weight.

(F) Mouse body weights of subcutaneous 8505C tumors.

(G) H&E staining of main organs, including heart, lung, liver, spleen, and kidney. Scale bar equals to 20 μm.

(H) blood chemistry parameters (ALT, AST, ALP, and Cre) measured when treated mice were sacrificed in different groups. One-way ANOVA was employed to compare tumor volume in different groups; *p < 0.05; **p < 0.01; ***p < 0.001.

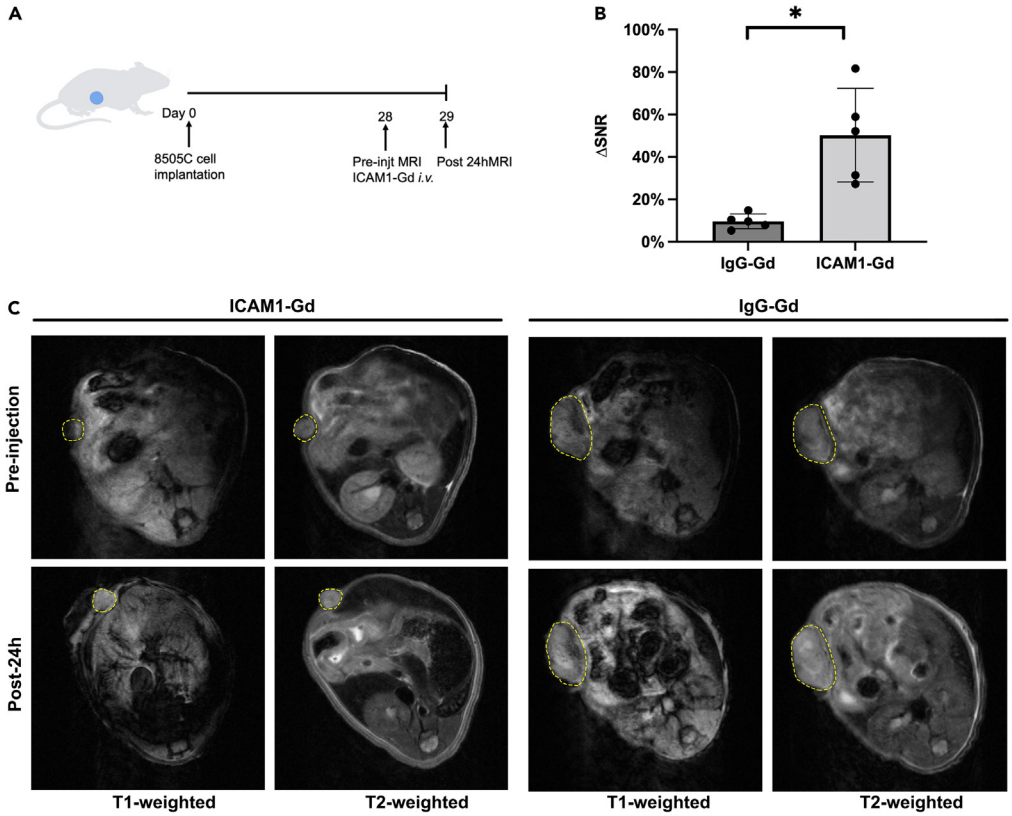

Figure 7. Assessment of ICAM1-expressing thyroid cancer by noninvasive MRI

(A) Schematic diagram of subcutaneous tumor model injected 8505C at Day 0, receiving ICAM1-Gd or IgG-Gd at 28 days post tumor inoculation (N = 5 per group) with MRI performed at Day29.

(B) Quantitative changes of MRI signal-to-noise ratio in thyroid cancer. Bar graphs are shown as mean ± SD. Students' T test was employed; *$p < 0.05$.

(C) Representative *in vivo* T1-and T2-weighted MR images of mice bearing subcutaneous tumor received ICAM1-Gd and IgG-Gd. The yellow arrows represent tumor.

group and I1-MMAE group. The serum biochemical parameters were quantified to further evaluate the toxicity of ADC. As is shown in Figures 6H and S3D, liver function (ALT, AST, ALP, and TB) and kidney function (Cre and BUN) were all within normal ranges in I1-DXd group and I1-MMAE group, indicating no evident off-target effects *in vivo*.

Noninvasive intratumoral biomarker evaluation by MRI

To build a precision medicine for thyroid cancer, we also developed an MRI-based molecular imaging approach to noninvasively and quantitatively detect intratumoral ICAM1 antigen evaluation.[14] We constructed an ICAM1-targeted MRI probe by conjugating ICAM1 antibody with DTPA-Gd, a clinically used MRI contrast agent. The non-targeting IgG-Gd was prepared as a negative control. ICAM1-Gd/IgG-Gd were administered into 8505C tumor-bearing mice at an intravenous dosage of 5 mg/kg (n = 5 per group). At pre-injection and 24 h post-injection of MRI probes, we performed *in vivo* MRI on tumor-bearing mice with a set of MRI sequences (Figure 7A). As is shown in Figure 7B, the signal/noise ratio (SNR) of post-injection increased 50.24% in comparison with the pre-injection SNR in ICAM1-Gd group (9.6%, $p = 0.013$), whereas no significant SNR changes was observed in the non-targeting IgG-Gd group. Since SNR changes positively correlates with intratumoral antigen expression, this MRI-based molecular imaging approach can be potentially used to identify ICAM1-positive patients who might benefit from ICAM1-ADC.

DISCUSSION

There is a rapidly increasing incidence of thyroid cancer in recent decades. Although most well-differentiated thyroid cancers are highly treatable, there are no effective therapies against advanced radioactive

iodine-resistant PTC.[26] The oral multi kinase inhibitors (sorafenib, Lenvatinib et al.) only improved progression-free survival instead of overall survival.[4,5] In addition, ATC do not respond to conventional treatments and lead to poor survival. These aggressive thyroid cancer subtypes represent an important unmet medical challenge and there is an urgent need to develop new treatment strategy for these patients.

To address this challenge, here we identified and evaluated ICAM1 as a promising ADC target for advanced PTC and ATC via bioinformatical analysis, unbiased target antigen screen and IHC. In addition, we engineered different ADC targeting ICAM1 and demonstrated their anti-thyroid cancer activity *in vitro* and *in vivo*. To our knowledge, this study is the first report to demonstrate the anti-tumor activity *in vivo* of ADC in thyroid cancer (PTC and ATC). We also designed a noninvasive MRI probe (ICAM1-Gd) as a precision medicine approach for thyroid cancer. Given the high specificity of ICAM1 in thyroid cancer and excellent anti-tumor activity *in vivo*, this study strongly supports these ICAM1-ADCs were promising targeted therapeutic candidates for devastating advanced PTC and ATC.

ICAM1 is a cell surface glycoprotein, belonging to the Ig superfamily. An ICAM1-targeted CAR-T showed potent anti-tumor activity against thyroid cancer in preclinical study.[13] Treatment of solid tumors with CAR-T cells is facing multiple complex obstacles, such as trafficking T cells to the tumor sites, the infiltration into hostile tumor microenvironment and immune-related toxicities.[27] On the other hand, ADCs have demonstrated clinically approved efficacy against multiple refractory and heterogeneous solid tumors owing to their superior tumor infiltration, unique bystander killing effect and higher tumor-selective potency, thus we selected ADC as our strategy to develop ICAM1-targeted therapeutic for advanced thyroid cancers.

In this study, we first demonstrated the overexpression of ICAM1 in PTC and ATC in different methods. High expression of ICAM1 is also a significant negative prognostic factor in thyroid cancer as demonstrated by TCGA data. Moreover, ICAM1 is significantly negatively associated with thyroid differentiation score, which is designated by TCGA working group with 16 genes.[19] The expression of ICAM1 in tall-cell variant (TCV) of PTC, as more aggressive subtype of PTC with a poor prognosis, is significantly higher than conventional PTC. The aforementioned data suggest that ICAM1 plays a potential role in the thyroid differentiation, aggressive phenotype, and prognosis. Next, we generated I1-MMAE-Cy5.5 to evaluate organ biodistribution of ICAM1-ADC. The results showed the I1-MMAE-Cy5.5 was not preferable in brain, lung, liver, heart, kidney, and targeted in tumor. We also synthesized a tumor-targeted molecular MRI contrast agent, which was constructed by the conjugation of Gd-DTPA to ICAM1. In the *in vivo* MRI study, the images on the 7.0T MR scanner showed that the tumor was enhanced clearly by Gd-DTPA-ICAM1. The analysis of quantitative changes of SNR in Gd-DTPA-ICAM1 was significantly higher than Gd-DTPA-IgG. The molecular probe Gd-DTPA-ICAM1 provides a clinically applicable diagnostic modality for precision therapy in thyroid cancer therapy.

ADCs have emerged as a new attractive treatment modality in oncology especially after the recent success of DS-8201 in HER2-amplified multi-cancers.[28–31] In this study, we designed two ADCs targeting ICAM1, with different cytotoxic agents (payload) and linker. Both ADCs shows objective anti-tumor activity *in vivo* and *in vitro*. The payload DXd as a DNA topoisomerase I inhibitor, and MMAE as a microtubule inhibitor, are clinically utilized ADC warheads. These two warheads manifest different intracellular processing and anti-tumor mechanism. Previous studies compared the activity of cell-free DNA topoisomerase I inhibitor (SN-38 and DXd) and revealed that DXd had a lower IC_{50} in treating cancer cells (IC_{50}: 2.78umol/L, 0.31umol/L, respectively).[32] The SN-38 had shown excellent anti-tumor efficacy in PTC and ATC in previous studies *in vivo* and *in vitro*.[33–36] The IC_{50} of SN-38 in 8505C was reported as 11.2–186.3 nM.[33,34] Besides, irinotecan, converted to its active metabolite SN-38, had shown anti-tumor efficacy in an insular thyroid carcinoma patient (who was resistant to doxorubicin and paclitaxel) in a case report.[37] DXd, with a better anti-tumor activity than SN-38, was firstly reported to shown anti-tumor efficacy in PTC and ATC in this study. MMAE, as the most commonly used cytotoxins in nearly one-third of clinical ADCs, was membrane-permeable and could improve response rate through bystander killing effect, with an IC_{50} of approximately 1 nM for all of the cell lines used. The results revealed the lower IC_{50} of MMAE in comparison with DXd *in vitro*. We also tested the anti-tumor activity of ICAM1-ADC *in vivo* and found both ICAM1 ADCs had significant advantages over conventional chemotherapy (paclitaxel). The mean tumor size in I1-DXd group was smaller than I1-MMAE group, but the difference was not significant.

In this study, we determined the potential of ICAM1 as a promising ADC target for advanced PTC and ATC by quantitatively determining its tumor specificity, tumor expression level, receptor-mediated internalization, ADC efficacy, and MRI-guided molecular imaging. We report here the first demonstration of anti-tumor efficacies of two ICAM1-ADCs in preclinical models of ATC and PTC. Moreover, we also developed an MRI-based molecular imaging probe Gd-DTPA-ICAM1 to guide ICAM1 ADC as a precision medicine. Owing to these encouraging experimental evidence, ICAM1-ADCs warrant further clinical investigations as promising ADC candidates for thyroid cancer.

Limitations of the study

Despite the promising nature of these results, there are several limitations in this study that need further investigation. Although the overexpression of ICAM1 in thyroid cancer was initially determined, the biological mechanism of ICAM1 overexpression has yet been elucidated in this study. In addition, preclinical studies including pharmacokinetics, dosage optimization, and biosafety of ICAM1-ADCs could provide more crucial information for its clinical translation. The patient-derived xenograft (PDX) model should be helpful to evaluate the treatment efficacy of ICAM1-ADC to heterogeneous thyroid cancer.

STAR★METHODS

Detailed methods are provided in the online version of this paper and include the following:

- KEY RESOURCES TABLE
- RESOURCE AVAILABILITY
  - Lead contact
  - Materials availability
  - Data and code availability
- EXPERIMENTAL MODEL AND STUDY PARTICIPANT DETAILS
- METHOD DETAILS
  - Immunohistochemistry (IHC) staining
  - Evaluating cell surface ICAM1 expression and its internalization
  - Immunofluorescent staining
  - Preparation and characterization of antibody–drug conjugates
  - Cell cytotoxicity of ADCs
  - Bioinformatics analysis
  - *In vivo* tumor targeting and biodistribution
  - Synthesis of MRI probe ICAM1-Gd
  - *In vivo* efficacy of ICAM1 ADCs
  - Blood chemistry and histology analysis
- QUANTIFICATION AND STATISTICAL ANALYSIS

SUPPLEMENTAL INFORMATION

Supplemental information can be found online at https://doi.org/10.1016/j.isci.2023.107272.

ACKNOWLEDGMENTS

The authors would like to thank Institute of Basic medicine and cancer (IBMC), Chinese Academy of Sciences for technical support. This study was supported by the National Natural Science Foundation of China (NSFC; 82172598), the Natural Science Foundation of Zhejiang Province, China (LZ22H310001), the 551 Health Talent Training Project of Health Commission of Zhejiang Province, China, the Agricultural and Social Development Research Project of Hangzhou Muncipal Science and Technology Bureau (2022ZDSJ0474), the Medical and Health Science and Technology Project of Zhejiang Province, China (2023RC134), Wujieping Science Foundation of China (no.320.6750.19094-46). All animal studies were performed according to the protocols approved by the Institutional Animal Care and Use Committee (IACUC) of Zhejiang Cancer Hospital (No.2022-07-016).

AUTHOR CONTRIBUTIONS

M.A.M., P.G., J.F., T.S., and P.Z. designed the work and wrote the paper. A.C.H., N.K., and Y.D.designed the antibody drug conjugates. P.Z., C.T., and S.Y. performed most of the experiments. Y.X. and X.W.

analyzed and supervised the immunohistochemical experiments. All authors read and approved the manuscript.

DECLARATION OF INTERESTS

P.Z. and P.G. are co-inventors of a patent application filed by Zhejiang Cancer Hospital. A.C.H and J.F. are shareholders of MabPlex. The other authors have declared no conflicts of interest.

Received: February 3, 2023
Revised: April 27, 2023
Accepted: June 28, 2023
Published: July 3, 2023

REFERENCES

1. Sung, H., Ferlay, J., Siegel, R.L., Laversanne, M., Soerjomataram, I., Jemal, A., and Bray, F. (2021). Global Cancer Statistics 2020: GLOBOCAN Estimates of Incidence and Mortality Worldwide for 36 Cancers in 185 Countries. CA. Cancer J. Clin. *71*, 209–249. https://doi.org/10.3322/caac.21660.

2. Miller, K.D., Nogueira, L., Devasia, T., Mariotto, A.B., Yabroff, K.R., Jemal, A., Kramer, J., and Siegel, R.L. (2022). Cancer treatment and survivorship statistics, 2022. CA. Cancer J. Clin. *72*, 409–436. https://doi.org/10.3322/caac.21731.

3. Cabanillas, M.E., McFadden, D.G., and Durante, C. (2016). Thyroid cancer. Lancet *388*, 2783–2795. https://doi.org/10.1016/S0140-6736(16)30172-6.

4. Schlumberger, M., Tahara, M., Wirth, L.J., Robinson, B., Brose, M.S., Elisei, R., Habra, M.A., Newbold, K., Shah, M.H., Hoff, A.O., et al. (2015). Lenvatinib versus placebo in radioiodine-refractory thyroid cancer. N. Engl. J. Med. *372*, 621–630. https://doi.org/10.1056/NEJMoa1406470.

5. Brose, M.S., Nutting, C.M., Jarzab, B., Elisei, R., Siena, S., Bastholt, L., de la Fouchardiere, C., Pacini, F., Paschke, R., Shong, Y.K., et al. (2014). Sorafenib in radioactive iodine-refractory, locally advanced or metastatic differentiated thyroid cancer: a randomised, double-blind, phase 3 trial. Lancet *384*, 319–328. https://doi.org/10.1016/S0140-6736(14)60421-9.

6. Falchook, G.S., Millward, M., Hong, D., Naing, A., Piha-Paul, S., Waguespack, S.G., Cabanillas, M.E., Sherman, S.I., Ma, B., Curtis, M., et al. (2015). BRAF inhibitor dabrafenib in patients with metastatic BRAF-mutant thyroid cancer. Thyroid *25*, 71–77. https://doi.org/10.1089/thy.2014.0123.

7. Hyman, D.M., Puzanov, I., Subbiah, V., Faris, J.E., Chau, I., Blay, J.Y., Wolf, J., Raje, N.S., Diamond, E.L., Hollebecque, A., et al. (2015). Vemurafenib in Multiple Nonmelanoma Cancers with BRAF V600 Mutations. N. Engl. J. Med. *373*, 726–736. https://doi.org/10.1056/NEJMoa1502309.

8. Modi, S., Jacot, W., Yamashita, T., Sohn, J., Vidal, M., Tokunaga, E., Tsurutani, J., Ueno, N.T., Prat, A., Chae, Y.S., et al. (2022). Trastuzumab Deruxtecan in Previously Treated HER2-Low Advanced Breast Cancer. N. Engl. J. Med. *387*, 9–20. https://doi.org/10.1056/NEJMoa2203690.

9. Drago, J.Z., Modi, S., and Chandarlapaty, S. (2021). Unlocking the potential of antibody-drug conjugates for cancer therapy. Nat. Rev. Clin. Oncol. *18*, 327–344. https://doi.org/10.1038/s41571-021-00470-8.

10. Bui, T.M., Wiesolek, H.L., and Sumagin, R. (2020). ICAM-1: A master regulator of cellular responses in inflammation, injury resolution, and tumorigenesis. J. Leukoc. Biol. *108*, 787–799. https://doi.org/10.1002/JLB.2MR0220-549R.

11. Nakashima, M., Eguchi, K., Ishikawa, N., Yamashita, I., Sakai, M., Ida, H., Kawabe, Y., Ito, K., and Nagataki, S. (1994). Expression of adhesion molecule ICAM-1 (CD54) in thyroid papillary adenocarcinoma. J. Endocrinol. Invest. *17*, 843–848. https://doi.org/10.1007/BF03347789.

12. Buitrago, D., Keutgen, X.M., Crowley, M., Filicori, F., Aldailami, H., Hoda, R., Liu, Y.F., Hoda, R.S., Scognamiglio, T., Jin, M., et al. (2012). Intercellular adhesion molecule-1 (ICAM-1) is upregulated in aggressive papillary thyroid carcinoma. Ann. Surg Oncol. *19*, 973–980. https://doi.org/10.1245/s10434-011-2029-0.

13. Min, I.M., Shevlin, E., Vedvyas, Y., Zaman, M., Wyrwas, B., Scognamiglio, T., Moore, M.D., Wang, W., Park, S., Park, S., et al. (2017). CAR T Therapy Targeting ICAM-1 Eliminates Advanced Human Thyroid Tumors. Clin. Cancer Res. *23*, 7569–7583. https://doi.org/10.1158/1078-0432.CCR-17-2008.

14. Guo, P., Huang, J., Wang, L., Jia, D., Yang, J., Dillon, D.A., Zurakowski, D., Mao, H., Moses, M.A., and Auguste, D.T. (2014). ICAM-1 as a molecular target for triple negative breast cancer. Proc. Natl. Acad. Sci. USA *111*, 14710–14715. https://doi.org/10.1073/pnas.1408556111.

15. Huang, J., Agoston, A.T., Guo, P., and Moses, M.A. (2020). A Rationally Designed ICAM1 Antibody Drug Conjugate for Pancreatic Cancer. Adv. Sci. *7*, 2002852. https://doi.org/10.1002/advs.202002852.

16. Yang, Y., Yang, H., Alcaina, Y., Puc, J., Birt, A., Vedvyas, Y., Gallagher, M., Alla, S., Riascos, M.C., McCloskey, J.E., et al. (2023). Inducible expression of interleukin-12 augments the efficacy of affinity-tuned chimeric antigen receptors in murine solid tumor models. Nat. Commun. *14*, 2068. https://doi.org/10.1038/s41467-023-37646-y.

17. Gray, K.D., McCloskey, J.E., Vedvyas, Y., Kalloo, O.R., Eshaky, S.E., Yang, Y., Shevlin, E., Zaman, M., Ullmann, T.M., Liang, H., et al. (2020). PD1 Blockade Enhances ICAM1-Directed CAR T Therapeutic Efficacy in Advanced Thyroid Cancer. Clin. Cancer Res. *26*, 6003–6016. https://doi.org/10.1158/1078-0432.CCR-20-1523.

18. Yang, Y., McCloskey, J.E., Yang, H., Puc, J., Alcaina, Y., Vedvyas, Y., Gomez Gallegos, A.A., Ortiz-Sánchez, E., de Stanchina, E., Min, I.M., et al. (2021). Bispecific CAR T Cells against EpCAM and Inducible ICAM-1 Overcome Antigen Heterogeneity and Generate Superior Antitumor Responses. Cancer Immunol. Res. *9*, 1158–1174. https://doi.org/10.1158/2326-6066.CIR-21-0062.

19. Cancer Genome Atlas Research Network (2014). Integrated genomic characterization of papillary thyroid carcinoma. Cell *159*, 676–690. https://doi.org/10.1016/j.cell.2014.09.050.

20. Cabanillas, M.E., Ryder, M., and Jimenez, C. (2019). Targeted Therapy for Advanced Thyroid Cancer: Kinase Inhibitors and Beyond. Endocr. Rev. *40*, 1573–1604. https://doi.org/10.1210/er.2019-00007.

21. Wagle, M.C., Kirouac, D., Klijn, C., Liu, B., Mahajan, S., Junttila, M., Moffat, J., Merchant, M., Huw, L., Wongchenko, M., et al. (2018). A transcriptional MAPK Pathway Activity Score (MPAS) is a clinically relevant biomarker in multiple cancer types. NPJ Precis. Oncol. *2*, 7. https://doi.org/10.1038/s41698-018-0051-4.

22. Tomás, G., Tarabichi, M., Gacquer, D., Hébrant, A., Dom, G., Dumont, J.E., Keutgen, X., Fahey, T.J., 3rd, Maenhaut, C., and Detours, V. (2012). A general method to derive robust organ-specific gene expression-based differentiation indices: application to thyroid cancer diagnostic. Oncogene *31*, 4490–4498. https://doi.org/10.1038/onc.2011.626.

23. Harper, J., Mao, S., Strout, P., and Kamal, A. (2013). Selecting an optimal antibody for antibody-drug conjugate therapy: internalization and intracellular localization.

Methods Mol. Biol. *1045*, 41–49. https://doi.org/10.1007/978-1-62703-541-5_3.

24. Kavanaugh, A.F., Davis, L.S., Jain, R.I., Nichols, L.A., Norris, S.H., and Lipsky, P.E. (1996). A phase I/II open label study of the safety and efficacy of an anti-ICAM-1 (intercellular adhesion molecule-1; CD54) monoclonal antibody in early rheumatoid arthritis. J. Rheumatol. *23*, 1338–1344.

25. Guo, P., Yang, J., Liu, D., Huang, L., Fell, G., Huang, J., Moses, M.A., and Auguste, D.T. (2019). Dual complementary liposomes inhibit triple-negative breast tumor progression and metastasis. Sci. Adv. *5*, eaav5010. https://doi.org/10.1126/sciadv.aav5010.

26. Higgins, M.J., Forastiere, A., and Marur, S. (2009). New directions in the systemic treatment of metastatic thyroid cancer. Oncology (Williston Park) *23*, 768–775.

27. Hong, M., Clubb, J.D., and Chen, Y.Y. (2020). Engineering CAR-T Cells for Next-Generation Cancer Therapy. Cancer Cell *38*, 473–488. https://doi.org/10.1016/j.ccell.2020.07.005.

28. Tamura, K., Tsurutani, J., Takahashi, S., Iwata, H., Krop, I.E., Redfern, C., Sagara, Y., Doi, T., Park, H., Murthy, R.K., et al. (2019). Trastuzumab deruxtecan (DS-8201a) in patients with advanced HER2-positive breast cancer previously treated with trastuzumab emtansine: a dose-expansion, phase 1 study. Lancet Oncol. *20*, 816–826. https://doi.org/10.1016/S1470-2045(19)30097-X.

29. Modi, S., Saura, C., Yamashita, T., Park, Y.H., Kim, S.B., Tamura, K., Andre, F., Iwata, H., Ito, Y., Tsurutani, J., et al. (2020). Trastuzumab Deruxtecan in Previously Treated HER2-Positive Breast Cancer. N. Engl. J. Med. *382*, 610–621. https://doi.org/10.1056/NEJMoa1914510.

30. Shitara, K., Bang, Y.J., Iwasa, S., Sugimoto, N., Ryu, M.H., Sakai, D., Chung, H.C., Kawakami, H., Yabusaki, H., Lee, J., et al. (2020). Trastuzumab Deruxtecan in Previously Treated HER2-Positive Gastric Cancer. N. Engl. J. Med. *382*, 2419–2430. https://doi.org/10.1056/NEJMoa2004413.

31. Li, B.T., Smit, E.F., Goto, Y., Nakagawa, K., Udagawa, H., Mazières, J., Nagasaka, M., Bazhenova, L., Saltos, A.N., Felip, E., et al. (2022). Trastuzumab Deruxtecan in HER2-Mutant Non-Small-Cell Lung Cancer. N. Engl. J. Med. *386*, 241–251. https://doi.org/10.1056/NEJMoa2112431.

32. Ogitani, Y., Aida, T., Hagihara, K., Yamaguchi, J., Ishii, C., Harada, N., Soma, M., Okamoto, H., Oitate, M., Arakawa, S., et al. (2016). DS-8201a, A Novel HER2-Targeting ADC with a Novel DNA Topoisomerase I Inhibitor, Demonstrates a Promising Antitumor Efficacy with Differentiation from T-DM1. Clin. Cancer Res. *22*, 5097–5108. https://doi.org/10.1158/1078-0432.CCR-15-2822.

33. Banchi, M., Orlandi, P., Gentile, D., Alì, G., Fini, E., Fontanini, G., Francia, G., and Bocci, G. (2020). Synergistic activity of linifanib and irinotecan increases the survival of mice bearing orthotopically implanted human anaplastic thyroid cancer. Am. J. Cancer Res. *10*, 2120–2127.

34. Di Desidero, T., Antonelli, A., Orlandi, P., Ferrari, S.M., Fioravanti, A., Alì, G., Fontanini, G., Basolo, F., Francia, G., and Bocci, G. (2017). Synergistic efficacy of irinotecan and sunitinib combination in preclinical models of anaplastic thyroid cancer. Cancer Lett. *411*, 35–43. https://doi.org/10.1016/j.canlet.2017.09.032.

35. Yu, T., Tong, L., Ao, Y., Zhang, G., Liu, Y., and Zhang, H. (2020). NIR triggered PLGA coated Au-TiO2 core loaded CPT-11 nanoparticles for human papillary thyroid carcinoma therapy. Drug Deliv. *27*, 855–863. https://doi.org/10.1080/10717544.2020.1775723.

36. Kim, S., Prichard, C.N., Younes, M.N., Yazici, Y.D., Jasser, S.A., Bekele, B.N., and Myers, J.N. (2006). Cetuximab and irinotecan interact synergistically to inhibit the growth of orthotopic anaplastic thyroid carcinoma xenografts in nude mice. Clin. Cancer Res. *12*, 600–607. https://doi.org/10.1158/1078-0432.CCR-05-1325.

37. Briasoulis, E., Rontogianni, D., Karavasilis, V., and Pavlidis, N. (2005). Oxaliplatin (Eloxatin) plus irinotecan combination chemotherapy found effective in refractory metastatic insular thyroid carcinoma. Thyroid *15*, 614–617. https://doi.org/10.1089/thy.2005.15.614.

38. Guo, P., Yang, J., Jia, D., Moses, M.A., and Auguste, D.T. (2016). ICAM-1-Targeted, Lcn2 siRNA-Encapsulating Liposomes are Potent Anti-angiogenic Agents for Triple Negative Breast Cancer. Theranostics *6*, 1–13. https://doi.org/10.7150/thno.12167.

39. Senter, P.D., and Sievers, E.L. (2012). The discovery and development of brentuximab vedotin for use in relapsed Hodgkin lymphoma and systemic anaplastic large cell lymphoma. Nat. Biotechnol. *30*, 631–637. https://doi.org/10.1038/nbt.2289.

40. Liao-Chan, S., Daine-Matsuoka, B., Heald, N., Wong, T., Lin, T., Cai, A.G., Lai, M., D'Alessio, J.A., and Theunissen, J.W. (2015). Quantitative assessment of antibody internalization with novel monoclonal antibodies against Alexa fluorophores. PLoS One *10*, e0124708. https://doi.org/10.1371/journal.pone.0124708.

41. Huang, J., Guo, P., and Moses, M.A. (2020). Rationally Designed Antibody Drug Conjugates Targeting the Breast Cancer-Associated Endothelium. ACS Biomater. Sci. Eng. *6*, 2563–2569. https://doi.org/10.1021/acsbiomaterials.9b01060.

42. Tang, Z., Li, C., Kang, B., Gao, G., Li, C., and Zhang, Z. (2017). GEPIA: a web server for cancer and normal gene expression profiling and interactive analyses. Nucleic Acids Res. *45*, W98–W102. https://doi.org/10.1093/nar/gkx247.

43. Chandrashekar, D.S., Karthikeyan, S.K., Korla, P.K., Patel, H., Shovon, A.R., Athar, M., Netto, G.J., Qin, Z.S., Kumar, S., Manne, U., et al. (2022). UALCAN: An update to the integrated cancer data analysis platform. Neoplasia *25*, 18–27. https://doi.org/10.1016/j.neo.2022.01.001.

44. Zhang, Y., Wang, M., Liu, W., and Peng, X. (2019). Optical Imaging of Triple-Negative Breast Cancer Cells in Xenograft Athymic Mice Using an ICAM-1-Targeting Small-Molecule Probe. Mol. Imaging Biol. *21*, 835–841. https://doi.org/10.1007/s11307-018-01312-3.

STAR★METHODS

KEY RESOURCES TABLE

REAGENT or RESOURCE	SOURCE	IDENTIFIER
Antibodies		
PE Mouse monoclonal anti-CD54	BioLegend	Cat#353106; RRID:AB_10897647
Mouse monoclonal purified anti- CD54	BioLegend	Cat#322702; RRID:AB_535974
PE Mouse IgG	BioLegend	Cat#400114;PRID: AB_10002181
Rabbit monoclonal anti-CD54	Sigma-Aldrich	Cat# HPA004877; RRID:AB_1846317
Critical commercial assays		
CCK8	APExBIO	Cat#K1018
Experimental models: Cell lines		
Human: BCPAP	Cell Culture Collection of the Chinese Academy of Sciences (Shanghai, China)	SCSP-543; Female; Braf V600E mutation; PTC cell line
Human: IHH4	JCRB	JCRB1079; Male; Braf V600E mutation; PTC cell line
Human: TPC1	ATCC	Female; Braf wild type; PTC cell line
Human: TCO-1	JCRB	JCRB0239; Sex NA; Braf wild type; ATC cell line
Human: 8505C	Cell Culture Collection of the Chinese Academy of Sciences (Shanghai, China)	SCSP-540; Female; Braf V600E mutation; ATC cell line
Human: ASH3	JCRB	JCRB1073; Female; Braf wild type; ATC cell line
Human:293T	ATCC	CRL-3216; Sex NA; Kidney epithelial cells
Experimental models: Organisms/strains		
BALB/c Nude mice	Kawensi biotech Co., Ltd	N/A
Software and algorithms		
Adobe Illustrator 2020	Adobe	https://www.adobe.com/
Adobe Photoshop 2020	Adobe	https://www.adobe.com/
GraphPad Prism 7.0	GraphPad	http://www.graphpad-prism.cn/?c=i&a=prism
SPSS 20.0	IBM	https://spss.en.softonic.com/
Other		
Thyroid tissue microarrays	OUTDO Biotech	N/A

RESOURCE AVAILABILITY

Lead contact

Further information and requests for resources and reagents should be contacted directly to and will be fulfilled by the Lead Contact, Peng Guo (guopeng@ucas.ac.cn).

Materials availability

This study did not generate new unique reagents.

Data and code availability

- All bioinformatic data sets used in this manuscript were obtained from publicly accessible GEO dataset and TCGA dataset as indicated in the method details.
- This paper does not report original code.
- Any additional information required to reanalyze the data reported in this paper is available from the lead contact upon request.

EXPERIMENTAL MODEL AND STUDY PARTICIPANT DETAILS

Human thyroid cancer cell lines BCPAP and 8505C were obtained from the Cell Culture Collection of the Chinese Academy of Sciences (Shanghai, China). Human thyroid cancer cell lines IHH4, TCO-1 and ASH3 were obtained from the Japanese Collection of Research Bioresources (JCRB) Cell Bank. Human thyroid cancer cell line TPC1 and normal human embryonic kidney 293T cells were obtained from American Type Culture Collection (Manassas, VA, USA). TCO-1, 8505C and TPC1 were cultured in DMEM. IHH4, BCPAP and HEK 293T were cultured in Roswell Park Memorial Institute (RPMI)-1640. ASH-3 was cultured in DMEM and RPMI-1640 (1:1), with all recommended supplements, respectively. All cells were maintained at 37°C in a humidified incubator with 5% (vol/vol) CO_2.

METHOD DETAILS

Immunohistochemistry (IHC) staining

IHC staining was conducted on paraffin-embedded human PTC, ATC and normal thyroid TMA purchased from OUTDO Biotech (Shanghai, China) for ICAM1 expression. The TMA involved 6 ATCs, 74 PTCs and 74 normal thyroid tissues. IHC staining of TMA was performed using a two-step method. After heat-induced antigen retrieval, the TMA was incubated with primary anti-ICAM1 antibody (1:1000; AB 1846317, Sigma-Aldrich) for 30 minutes at room temperature, followed by incubation with a matched secondary antibody for 30 minutes. The individual tissue cores in the TMA were scored by a pathologist, who was blinded to sample identity information, for no staining (0+), weak staining (1+), moderate staining (2+), or strong staining (3+). Each intensity category was scored as a percentage of tumor cells, which ranged from 0 to 100, so that the sum of the percentages adds up to 100. The percentage score was then multiplied by its intensity category to obtain a final "hybrid (H) score,", which ranged from 0 to 300.

Evaluating cell surface ICAM1 expression and its internalization

Cell surface ICAM1 expression levels were measured using Beckman Coulter's CytoFLEX LX Flow Cytometer as previously reported.[14,25,38] Briefly, 10^6 cells were collected and rinsed twice via suspension–spin cycles with cold PBS and blocked with 1% bovine serum albumin (BSA) for 30 min in an ice bath. After BSA blockage, cells were incubated with ICAM1 antibodies (Cat 353106, BioLegend, San Diego, CA) for 1 hour at room temperature. Stained cells were rinsed with a PBS buffer containing 1% BSA three times, resuspended in PBS for flow cytometry. As previously reported by us, the quantum simply cellular microbeads kit (Bangs Laboratories, IN, USA) was applied to quantify the cell surface expression of ICAM1 on various cancer cell lines.[25]

In the internalization experiment, 10^6 cells were first incubated with unconjugated mouse anti-human ICAM1 antibodies (Cat 322702, BioLegend, San Diego, CA) for 30min in an ice bath. The stained cells were rinsed with a PBS buffer containing 1% BSA and resuspended in PBS. The primary ICAM1 antibodies bound on cell membranes were allowed to be internalized for different time points (0min, 30 min, 60min, 120min, 240min). A secondary PE-conjugated rat anti-mouse IgG (BioLegend, San Diego, CA) was added to the stained cell for 30min and then rinsed by PBS, fixed by paraformaldehyde (4%) for flow cytometry. The internalization efficiency was calculated by an established formula (1-mean cell fluorescence intensity (t=incubation time)/mean cell fluorescent intensity(t=0min))×100%.[39,40] The internalization curve was generated by internalization efficiency at different time points.

Immunofluorescent staining

PE conjugated ICAM1 antibody (Santa Cruz Biotechnology, sc-107) was incubated with thyroid cancer cells at 37 °C for 45min, then washed with cold PBS, fixed with 4% paraformaldehyde, and blocked by 1% BSA, and analyzed by confocal microscopy. For internalization experiments, cancer cells were incubated with PE conjugated ICAM1 antibody for different time points (0min, 30min, 60min, 120min, 240min), then processed and analyzed as described above. Cell nuclei were counterstained with Hoechst 33258 in PBS for 10 minutes at room temperature. The stained cells were visualized by using a fluorescence microscope (Nikon A1 HD25; Nikon, Japan).

Preparation and characterization of antibody–drug conjugates

The payloads of the two ICAM1-ADCs were Monomethyl auristatin E(MMAE) and deruxtecan (DXd) respectively. I1-MMAE and I1-DXd were prepared (GLP grade) by MabPlex (Yantai, China) via covalently conjugated ICAM1 antibody (R6.5c, GeneScript) with ADC linker and payload combinations

(MC-VC-PAB-MMAE or MC-GGFG-DXd).[41] The DAR of I1-MMAE and I1-DXd was measured by using hydrophobic interaction chromatography.

Cell cytotoxicity of ADCs

Human thyroid cancer cells were seeded in a 96-well plate at a density of 3000 cells per well overnight. The cell culture medium was replaced with the medium containing either chemo drugs (maximum concentration: 117.11 μmol/L) or ICAM1-ADCs at serial diluted concentrations (maximum concentration: 0.67 μmol/L). After 96h, cell cytotoxicity was determined by using a CCK-8 kit (KeyGEN Biotech, China) following the manufacturer's protocol. The absorbance at 450 nm was measured with an ELISA browser (Bio-Tek EL 800, USA). The experiments were repeated three times.

Bioinformatics analysis

The gene expression datasets were obtained from GEO (http://www.ncbi.nlm.nih.gov/geo) to study the expression profiles of thyroid cancer. The inclusion criteria for the gene expression datasets were as follows: (a) samples containing thyroid cancer and normal thyroid tissues, (b) Homo sapiens as the organism. Based on the inclusion and exclusion criteria, three datasets GSE3467, GSE33630 and GSE50901 were selected for PTC. Three datasets GSE33630, GSE53072 and GSE65144 were selected for ATC.

For analysis of PTC, GSE3467 consisted 9 PTC and 9 normal thyroid samples, GSE33630 consisted 49 PTC and 45 normal thyroid samples, GSE50901 consisted 61 PTC and 4 normal thyroid samples. For analysis of ATC, GSE33630 consists of 11 ATC and 45 normal thyroid samples, GSE53072 consists of 5 ATC and 4 normal thyroid samples, GSE65144 consisted 12 ATC and 13 normal thyroid samples.

The GEO online tool GEOR2 was used to find the differentially expressed genes (DEGs) between thyroid cancer and normal thyroid tissue. Adjusted P-value (Adj.P) < 0.05 and |log2 fold-change (FC)| > 1.8 were used as thresholds for DEG identification. The protein-protein interaction (PPI) analysis of the identified DEGs was performed according to the Search Tool for the Retrieval of Interacting Genes (STRING; version 11.0, URL: https://string-db.org/) database and visualized using Cytoscape (version 3.7.1, https://cytoscape.org/download.html). Subsequently, the Cytoscape plug-in, cytohubba (version 0.1, URL: apps.cytoscape.org/apps/cytohubba), was used for hub gene identification. Hub genes were selected from the intersection of the top 10 genes calculated using 12 different topological analysis methods.

Data from The Cancer Genome Atlas (TCGA; https://cancergenome.nih.gov/) was used as an external validation dataset. The expression level of ICAM1 and follow-up clinical information of thyroid cancer patients were obtained from The Cancer Genome Atlas (TCGA) database. The analyses were performed at the GEPIA (Gene Expression Profiling Interactive Analysis, http://gepia.cancer-pku.cn/) platform and ULCAN (The University of ALabama at Birmingham CANcer data analysis Portal, http://ualcan.path.uab.edu/index.html) platform.[42,43]

In vivo tumor targeting and biodistribution

All animal studies were performed according to the protocols approved by the Institutional Animal Care and Use Committee (IACUC) of Zhejiang Cancer Hospital.

BALB/C nude mice (female, 4-6 weeks) were used establish subcutaneous PTC or ATC mouse tumor model. Mice were anesthetized by isoflurane, and 3×10^6 8505C (ATC) or IHH4 (PTC) cells mixed with growth factor-reduced matrigel (BD Biosciences) (1:1) were subcutaneously injected into the right flank of mice. The tumor-bearing mice were randomized into two groups (n=3 per group) and were intravenously injected IgG-Cy5.5 or ICAM1-MMAE-Cy5.5 at a dosage of 5mg/kg mouse weight. At 48h post injection, *in vivo* NIR fluorescence imaging was performed using an IVIS Lumina III imaging system (Caliper, Hopkinton, MA, USA). After *in vivo* NIR imaging, mice were sacrificed and their excised organs (brain, heart, liver, lung, kidney, spleen, and tumor) was re-measured using the IVIS Lumina III system.

Synthesis of MRI probe ICAM1-Gd

Two MRI probes (IgG-DTPA-Gd and ICAM1-DTPA-Gd) were prepared.[15,44] Briefly, the ICAM1 antibody (R6.5c, GeneScript) or IgG (AG-0052, Beijing Dingguo Changsheng Biotech, Co., Ltd., China) and DTPAA (2:1, mol/mol) was slowly added to NaHCO3 solution (pH 9.0, 0.1 M), and the mixture was rotated

for 24h at room temperature overnight. The reaction mixture was then dialyzed against ddH2O [molecular weight cut-off (MwCo) 3500] for 24h and the purified ICAM1-DTPA and IgG-DTPA were obtained. The ICAM1-DTPA or IgG-DTPA and GdCl3.6H2O were mixed in 0.1 M citrate buffer (pH 6.5) for 24h at a molar ratio of 1:1. The reaction liquid was dialyzed (MwCo 3500) for 24 h, and the water was changed every 3 h. The purified ICAM1-DTPA-Gd and IgG-DTPA-Gd were lyophilized to a powder and stored for subsequent use. The MRI experiments were performed by the Bruker Biospec (7.0 T) small animal MR system (BrukerBioSpin MRI, Ettlingen, Germany) using T2WI and T1WI sequences.[15]

In vivo efficacy of ICAM1 ADCs

The subcutaneous mouse tumor model was established as described above. Then the tumor-bearing mice were randomly divided into 5 groups ($n \geq 5$ per group) and received treatment of PBS, paclitaxel, ICAM1 antibody, I1-MMAE or I1- DXd at an equivalent dosage of 5 mg/kg per week via tail vein injection. Tumor growth was monitored twice weekly by two-dimensional measurements using a vernier caliper. Three times per week, the weight and size of the tumor were monitored. Animals were also monitored closely for signs of discomfort or pain. Tumor volume was estimated according to the formula: tumor volume (mm^3) = tumor $width^2 \times$ tumor length$\times 0.5$. Animals were euthanized at the end of the study, or when tumors reached 1500 mm^3.

Blood chemistry and histology analysis

The major organ from different groups were embedded in paraffin, cut into 4-μm-thick sections and stained with hematoxylin and eosin (H&E). Subsequently, bright-field images of the H&E-stained tissues were taken using SlideView VS200 (Olympus, Japan) for histological examination. The serum levels of alanine aminotransferase (ALT), aspartate aminotransferase (AST), alkaline phosphatase (ALP), total bilirubin (TB), blood concentration of creatinine (BUN) and creatinine (Cre) were determined with biochemical analyzer Hitachi-7180 (Hitachi, Yokohama, Japan).

QUANTIFICATION AND STATISTICAL ANALYSIS

Quantitative data are presented as means ± SD. Two-tailed Student's t test was applied when comparing two means. When comparing more than two means, ANOVA was used for multiple comparisons. Statistical analysis was performed using SPSS Statistics version 20.0 (IBM Corp, Armonk, NY, USA) or Prism 9.0 (Graph Pad Software Inc.). P values < 0.05 were considered statistically significant.